Development of an open-source segmented blade design tool

Benjamin Anderson[1], **Pietro Bortolotti**[1] **and Nick Johnson**[1]
[1]National Renewable Energy Laboratory, Golden, CO, USA
E-mail: benjamin.anderson@nrel.gov

Abstract. As wind turbines continue to grow ever larger to reduce the cost of energy, their blades follow suit, with the largest commercial offshore blades extending past 100 m. Massive blades such as these raise key transportation and manufacturing challenges, especially for land-based turbines. Segmented blades are one solution and are garnering increased industry and research interest. In this work, a detailed mechanical joint model is integrated into the Wind-Plant Integrated System Design and Engineering Model (WISDEM®), which will facilitate future segmented blade research and optimization. WISDEM is used to design a wind turbine with 100-m segmented blades. This wind turbine design is compared to other machines with 100-m monolithic blades designed for rail-transportability. The designs are compared in terms of blade mass and cost, turbine capital cost, annual energy production, and levelized cost of energy, with monolithic designs being the lightest and most economical. However, this result may vary by wind plant location. A variety of segmentation joint types exist, and they will inevitably vary in parameters such as cost, spanwise location, and physical characteristics. This work examines the sensitivity of wind turbine design drivers and annual energy production to a variety of the aforementioned parameters, using the open-source wind turbine design codes OpenFAST and WISDEM, finding that joint mass, stiffness, and location can have significant effects on design drivers.

1. Introduction

As wind turbines continue to grow ever larger in an effort to reduce the cost of energy, their blades follow suit, with the largest offshore commercial blades extending past 100 m. The Big Adaptive Rotor (BAR) project, sponsored by the U.S. Department of Energy, aims to develop technology to enable land-based blades over 100 m in length. Massive blades such as these raise key manufacturing and transportation challenges. Manufacturing costs climb steeply for large blades [1], and blade factories may reach their maximum length and height for blade production.

There are several key transportation challenges as well: blade length, width, and height are the three main constraints. Today, most land-based wind turbine blades are transported via road or rail. For both, routes need to be analyzed to assure that the blade has the necessary clearance; access to certain areas can be limited. For blades over 45 m long, oversize and overweight trucks with rear steering and escort vehicles are required, significantly raising costs. For blades over 61 m long, costs rise nonlinearly [2]. Finally, a "bounding box" around the height and width of the blade, determined by the blade's root diameter, maximum chord length, pre-bend, and pre-curve, must be cleared for transportation. This constraint is an issue with narrow roadways and lower bridges and can further limit viable transportation routes, increasing cost [1]. Given these

manufacturing and transportation difficulties, segmented blades are a viable option. Smaller blade segments can be manufactured and transported separately, then assembled on-site at the destination wind farm, overcoming the aforementioned issues with large monolithic blades. Other solutions, such as large monolithic rail-transportable blades, are also being researched [3].

The BAR project has considered several segmentation strategies, including inflatable blades [4] and spanwise joints. The latter strategy reduces the length of the blade segments, easing manufacturing and transportation. Challenges with spanwise joints include dividing the structural spar, which requires large loading to be handled by the joint, and finding the optimal segmentation location and joint type. Concerns include increased complexity, reliability, and on-site assembly costs. Various types of spanwise joints have been proposed: mechanical, adhesive, cable, and transverse fastener. Despite promising simulation results for adhesive joints [5], the majority of research has been performed on mechanical spanwise joints, and all commercial segmented blade implementations have used mechanical spanwise joints. As such, they will be the focus of this paper.

Qin et al. [6] developed a method to determine spanwise joint location based on structure, vibration, manufacturing, and assembly performance, and made several key observations: Choosing a relatively uniform blade thickness/chord location for the joint eased manufacturing and assembly. Modal excitation was promoted for midpoint and blade-tip joints, regardless of blade size, and could be somewhat mitigated by controls. Connection strength was most critical at the midpoint, which experienced high loading at a smaller cross section than the root. These factors together pushed the joint location toward the root, resulting in an optimal interval around 20% of the blade span. Other authors [7, 8, 9] have suggested joint locations up to 50% of the blade span, which is optimal for transportation considerations. Many experimental and commercial segmented blades have joint locations over 50% of the blade span. These locations require smaller, lighter, less expensive joints. As such, there is no agreed-upon optimal location.

Post et al. [10] developed a 61.5-m segmented blade design with highly detailed cost models, but the joint design was not detailed. The performance and economics of large segmented blades must be compared to other large monolithic blade types, such as upwind and downwind flexible blades, to determine their scaling potential. Bortolotti et al. [3] performed such research with the open-source tools OpenFAST [11] and the Wind-Plant Integrated System Design and Engineering Model (WISDEM®) [12], creating detailed designs of 100-m monolithic and segmented blades and comparing their performance under a variety of conditions. They found that flexible, rail transportable blades can be lighter and less expensive than segmented blades. However, they used a very simplified point-mass joint model, did not design the joint, and neglected transportation costs.

Segmented blade technology is maturing and may play a vital role in wind turbine advancement. Joint technology will inevitably vary, and the effect of joint parameters such as mass, inertia, stiffness, and cost on overall economics should be considered. For a more accurate comparison of the performance and economics of segmented and monolithic blades at various sizes, a detailed, open-source joint design model is proposed. The presented work is separated into three tasks: (1) integrate a segmented blade joint design model into the open-source WISDEM framework and use it to design an optimized 100-m segmented blade, (2) use WISDEM to complete a techno-economic comparison between turbine designs with 100-m segmented and monolithic blades, and (3) find the sensitivity of blade design drivers and annual energy production (AEP) to joint mass, inertia, stiffness, location, and cost.

2. Joint design model

2.1. Model overview

The joint design code models an embedded bushing joint, consisting of a bolt embedded in a half-threaded insert. The insert is glued to holes bored into the spar caps,

connects the two blade segments together, and is held in compression by the bolt. The spar cap is enlarged to accommodate the joint. The model solves for the number of bolts and spar cap dimensions needed to resist various loads at the joint station. Figure 2 displays a cross-sectional view of the model, along with top and side views of half of the modeled embedded bushing joint.

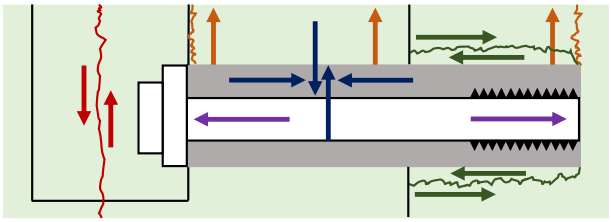

Figure 1. Side view of one bolt/insert pair in a spar cap side, showing failure modes considered: bolt tensile failure, insert von Mises yield, insert shear-out through top or bottom of spar cap side, insert pull-through, and spar cap shear at bolt-head hole.

2.2. Model calculations

2.2.1. Inputs and outputs

The model inputs are blade geometry, ultimate loads and fatigue damage equivalent loads (DELs) at the joint station, and joint bolt size. Flapwise and edgewise moments and forces are considered. The failure modes considered are displayed in figure 1. The model outputs the mass adder due to bolts, inserts, adhesive, and spar cap cutouts; costs from bolts, inserts, and adhesive; and required spar cap width and thickness to accommodate the joint.

2.2.2. Assumptions and constraints

Assumptions:

- Each spar cap side bears half of the load at the joint station. This is a simplification of reality, wherein the distance from a bolt to the neutral axis, which may not coincide with the chord, will determine its loading.
- Each spar cap side contains a single line of bolts, each separated by three bolt diameters.
- The spar cap sides are assumed to be on parallel lines to the chord, which is halfway between them, separated by a distance equal to the airfoil thickness minus the spar cap thickness. In reality, spar cap sides may not be straight lines.
- Flapwise loads are the joint design driver.
- Bolts are only in tension, taking no shear forces (due to preload). Inserts experience both normal and shear forces. Bolts and inserts may fail due to ultimate or fatigue loads.
- Torsion in the joint is not considered.
- The spar cap will not fail in fatigue, and is more likely to fail in shear than in tension, as it is a composite. The spar cap may fail by shear through bolt pull-through (in a spanwise direction), bolt shear-out (out the top/bottom of the spar cap), or at the bolt-head hole.

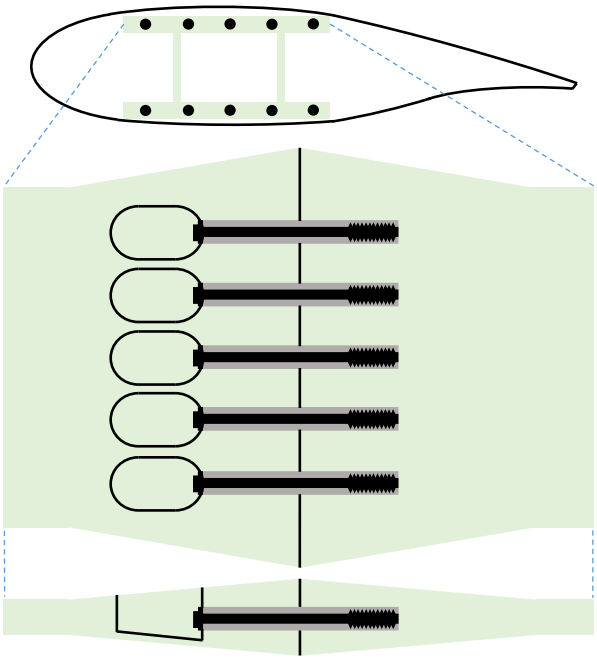

Figure 2. (Top) Cross-sectional view of the modeled embedded bushing joint, showing insert holes on spar cap pressure and suction sides. (Bottom) Top and side views of half of the modeled embedded bushing joint, consisting of a spar cap, inserts, and bolts. Each insert is held in compression by a bolt and is glued to the root and tip sections of the spar cap, which is enlarged to support the joint.

- Adhesive failure is not considered.

Constraints:

- The bolt line must be $\leq 80\%$ of the chord length due to transportation constraints. If more bolts are required, an error is returned.
- The spar cap must not extend more than 80% of the distance from the pitch axis to the leading and trailing edges. If it does, the spar cap is shifted toward the center of the blade section at that station.

2.2.3. Forces, joint properties, and minimum number of bolts
All joint load calculations are based on *Shigley's Mechanical Engineering Design* [13] unless otherwise stated. First, the code calculates the bolt and insert stiffness, k_{bolt} and k_{ist}, which are used to find the joint stiffness constant, C, by

$$C = \frac{k_{bolt}}{k_{bolt} + k_{ist}}, \quad \text{with} \quad k_{bolt} = \frac{A_d A_t E_{bolt}}{(A_d L_t + A_t L_d)}, \quad k_{ist} = \frac{A_{ist} E_{ist}}{L_{bolt}} \tag{1}$$

where A_d is bolt shank area, A_t is bolt thread area, E_{bolt} is bolt Young's modulus, L_t is thread length, L_d is shank length, A_{ist} is insert area, E_{ist} is insert elastic modulus, and L_{bolt} is bolt length. Next, the model initializes the joint preload to 70% of the bolt proof strength. The number of bolts required is calculated so that maximum axial bolt forces from flapwise moments are greater than those due to edgewise moments, and sets it as the minimum bolt number. This allows the rest of the design to be driven by ultimate flapwise loads, which in conventional wind turbine blades are greater in magnitude than edgewise loads. As such, axial and shear ultimate and fatigue joint forces per spar cap side are calculated by:

$$F_{ax,ult} = \frac{M_{flap,ult} k_l}{d_{sc}}, \quad F_{ax,fat} = \frac{M_{flap,DEL} k_l}{d_{sc}}, \quad F_{sh,ult} = \frac{F_{flap,ult} k_l}{2}, \quad F_{sh,fat} = \frac{F_{flap,DEL} k_l}{2} \tag{2}$$

where k_l is the input load multiplier recommended by International Electrotechnical Commission (IEC) standard 61400-1, d_{sc} is the distance between spar cap sides, $M_{flap\ ult}$ is the ultimate flap moment, $F_{flap\ ult}$ is the ultimate flap force, $M_{flap\ DEL}$ is the flap moment fatigue DEL, and $F_{flap\ DEL}$ is the flap force fatigue DEL.

2.2.4. Required number of bolt/insert pairs
Next, the model determines the number of bolts required to satisfy the constraints. It loops through the following calculations until the number of bolts converges to within 0.1 bolt. If the model does not converge, it takes the maximum of the last three bolt numbers calculated. A discrete mode was added, requiring an integer number of bolts, but for the sake of the optimizer, a continuous number of bolts is used. First, the loop calculates the number of bolts needed to resist ultimate axial loads, $n_{bolt\ ult}$, by:

$$n_{bolt,ult} = \frac{C F_{ax,ult}}{\frac{S_{p,bolt} A_t}{n_{prf}} - F_i} \tag{3}$$

where $S_{p,bolt}$ is bolt proof strength, n_{prf} is bolt proof safety factor, and F_i is bolt preload. Next, the loop calculates the number of inserts, n_{ist}, required to resist von Mises stress from axial and shear loads by solving the following system of equations:

$$\tau_{ist} = \frac{F_{sh,ult}}{A_{ist} n_{ist}}, \quad \sigma_{ist} = \frac{(1-C) F_{ax,ult}}{A_{ist} n_{ist}} + \frac{F_i}{A_{ist}}, \quad \sqrt{\sigma_{ist}^2 + 3\tau_{ist}^2} = \frac{S_{y,ist}}{n_y} \tag{4}$$

where τ_{ist} is insert shear stress, σ_{ist} is insert compressive stress, $S_{y,ist}$ is insert yield strength, A_{ist} is insert cross-sectional area, and n_y is yield safety factor. Next, the model calculates the number of bolts required to resist axial fatigue loads, $n_{bolt,fat}$, using a Goodman fatigue formulation:

$$n_{bolt,fat} = n_f \frac{\sigma_{a,bolt}}{S_{a,bolt}}, \quad \text{with} \quad \sigma_{a,bolt} = \frac{F_{ax,fat}C}{A_t}, \quad \sigma_{i,bolt} = \frac{F_i}{A_t}, \quad S_{a,bolt} = S_{e,bolt}(1 - \frac{\sigma_{i,bolt}}{S_{u,bolt}}) \tag{5}$$

where $S_{e,bolt}$ is bolt endurance strength, $S_{u,bolt}$ is bolt ultimate strength, $\sigma_{i,bolt}$ is bolt prestress, $\sigma_{a,bolt}$ is bolt stress amplitude, and n_f is fatigue safety factor. Next, the model calculates the number of inserts required to resist von Mises stress from axial and shear fatigue loads, $n_{ist,fat}$, using a Goodman fatigue formulation:

$$n_{ist,fat} = \left(\frac{n_f}{S_{a,ist}}\right)^{\frac{1}{2}} \left(\left(\frac{F_{ax,fat}(1-C)}{A_{ist}}\right)^2 + 3\frac{F_{sh,fat}}{A_{ist}}^2\right)^{\frac{1}{4}}, \quad \text{with} \quad S_{a,ist} = S_{e,ist}\left(1 - \frac{\sigma_{i,ist}}{S_{u,ist}}\right) \tag{6}$$

where $\sigma_{i,ist}$ is insert prestress, $S_{e,ist}$ is insert endurance strength, $S_{u,ist}$ is insert ultimate strength, and $S_{a,ist}$ is insert stress amplitude. Next, the number of inserts needed to resist axial pull-out through the spar cap is calculated by:

$$n_{bolt,pullout} = \frac{2n_s F_{ax,ult}}{(S_{s,sc}\pi(d_{ist} + 2t_{adhesive}))} \tag{7}$$

where n_s is shear safety factor, $S_{s,sc}$ is spar cap shear strength, d_{ist} is insert diameter, and $t_{adhesive}$ is adhesive thickness. Next, the model takes the maximum of these as the required number of bolt/insert pairs, n_{bolt}. Finally, the model calculates the preload required to prevent bolt separation, $F_{i,sep}$ and the bolt experiencing any shear forces, $F_{i,sh}$ by:

$$F_{i,sep} = \frac{n_0}{n_{bolt}} F_{ax,ult}(1-C), \quad F_{i,sh} = \frac{F_{sh,ult}}{\mu n_{bolt}} \tag{8}$$

where n_0 is the separation safety factor and μ is the frictional coefficient between spar cap sides. The preload is limited to 70% of the bolt proof load to prevent overloading.

2.2.5. Spar cap dimensions and mass calculations

After the number of bolts is determined, the model calculates the spar cap thickness required to resist loads. Fatigue is currently neglected in the spar cap. Shear forces are the design driver due to the isotropy of carbon and glass fibers, which typically make up spar cap materials. Shear-out of the insert and shear at the bolt-head holes are considered (both in the flapwise direction due to flapwise forces). The spar cap thickness needed to prevent insert shear-out and bolt-head hole shear are calculated by the following equations:

$$t_{sh,out} = \frac{2F_{sh,ult}n_s}{L_{ist}n_{bolt}S_{s,sc}}, \quad t_{sh,hole} = \frac{F_{sh,ult}n_s}{sS_{s,sc}n_{bolt}} + \frac{w_{hole}h_{hole}}{s} \tag{9}$$

where L_{ist} is insert length, s is bolt spacing, and w_{hole} and h_{hole} are the width and height of the bolt-head hole, respectively. Spar cap required width is calculated to accommodate the needed number of bolts. Next, the added mass of the joint, which is the sum of the mass of the bolts, inserts, and adhesive minus the mass of the displaced spar cap material, is calculated. Finally, the cost of these components is calculated. Material costs are calculated by mass. Mass and cost associated with the increased spar cap size are automatically calculated in a separate WISDEM rotor cost module [12].

2.3. WISDEM integration

The segmented blade joint design model described herein has been fully coupled with the WISDEM workflow. To model a wind turbine with segmented blades, the user specifies the joint location, bolt size, cost adder (to account for added manufacturing, assembly, and transportation costs), and joint material data as inputs. The joint model calculates required spar cap thickness, which the WISDEM optimizer can use as a constraint. Joint mass and cost are added as WISDEM outputs. One limitation of the current implementation hides in the steady-state nature of WISDEM, which is not able to compute DELs. In this project, DELs have been estimated using the simplified approaches presented in Bortolotti et al. [14].

3. Case study: Optimized BAR-USC II design in WISDEM

3.1. Optimization setup

A case study is presented that highlights the ability of the joint design model coupled with WISDEM to optimize a wind turbine with segmented blades. The case study focuses on the following question: What joint location is optimal, in terms of blade mass and cost? WISDEM can be run as an optimizer that uses design variables as inputs, a merit figure to minimize, and constraints to enforce. More details can be found in its documentation [12]. This study is focused on optimizing the blade structure and 30 design variables that control spar cap thickness, which is parameterized along the blade span at 30 uniformly distributed stations. The spar cap thickness is set the same between pressure and suction sides of the blade. To keep the aerodynamics the same as the baseline, the outer shape of the blade is not changed: the joint must fit within the given blade cross section. This analysis begins with a joint located at 70% of the blade span, as used in the prior study [3], and M36 bolts. Blade mass is used as the merit figure. Metric bolts with varying diameters (24, 30, 36, 42, 48, and 52 mm) are considered. Smaller bolts are found to yield lower blade mass and cost, so the smallest possible bolts are used for each station. This is limited by the number of bolts that can fit in a single line in the spar cap cross section, so larger bolts are needed as the joint moves toward the root. With the optimization parameters chosen, joint location is varied between 20% and 80% of the blade span in steps of 10%, and the blade mass and cost are compared for each optimization. Finally, a segmented blade design is compared to other monolithic designs.

3.2. Baseline designs

The baseline designs used in this study were developed by Bortolotti et al. [3]. The turbines are class IIIA, with $U_{avg} = 7.5$ m/s; each has different blade types but all have 100-m blade lengths. The three most promising designs all have carbon fiber spar caps, and include downwind (BAR-DRC) and upwind (BAR-URC) monolithic blades, which could be transported on rail via controlled flexing, along with an upwind segmented blade (BAR-USC). The BAR-USC's joint was originally modeled as a 2,000-kg point mass with a cost adder of $50,000, located at 70 m along the blade. The optimized designs are based on the BAR-USC (without the point mass and cost) and are called the BAR-USC II designs.

3.3. Joint cost adders

Transportation and manufacturing cost models are critical to finding turbine cost, but are notoriously difficult to obtain in the public domain. WISDEM does not include a blade transportation cost model at the time of writing. Smith et al. [15] examined pathways for supersized blades, including segmentation. They found that the transportation costs of segmented blades vary significantly depending on the assumptions chosen, including where the blade is manufactured, where it is being transported, the length of the blade, and the number of segments. Based on their results for a 95-m blade with a chordwise and a spanwise joint, transportation costs ranged from $17,000 less to $5,000 more per blade, relative to monolithic

blade transport. For the purposes of this study we choose a transportation savings, relative to monolithic blade transportation, of $10,000 per blade. Considering that the BAR-USC does not have a chordwise joint, this is likely conservative for most cases. This savings is used for all joint locations considered, as Smith et al. found that, although segmenting in the middle reduces expense per transport vehicle, segmenting at other locations could allow multiple, shorter segments to be transported on a single vehicle.

Post et al. [10] calculated joint manufacturing and assembly costs for a 61.5-m blade with 23.5-m tip length using a detailed, process-based model. They scaled their results up to a 104-m blade with 39.7-m tip length. While material costs increased significantly for the larger joint, other manufacturing and assembly costs (labor, tooling, and facility costs) only increased by about 7.6%. We interpolate linearly to find our joint nonmaterial manufacturing and assembly costs. The joint model in WISDEM calculates the material cost of the joint, which varies more significantly. Summing the transportation (-$10,000) and nonmaterial manufacturing and assembly costs, the joint cost adder ranges from 2.3% of total blade cost for a 90% span joint to 3.4% of total blade cost for a 20% span joint.

3.4. Case study results

The optimization finds that an outboard joint is most desirable in terms of blade mass and cost, as displayed in figure 3. Results are presented in terms of tip section length (blade length minus joint location) to highlight their generalizability to different segmented blade lengths. The size of the joint is driven by blade moments, which decrease from root to tip. So, WISDEM finds smaller, lighter, less expensive joints with increasing spanwise location. As shown in figure 3, changes in joint mass and material cost are larger than changes in overall blade mass and cost, respectively. This is because the increased spar cap thickness and stiffness of the joint location allows WISDEM to reduce spar cap thickness and stiffness elsewhere. The majority of the change in overall turbine mass and cost comes from the change in blade mass and cost. The optimization doesn't change the blade's outer shape, and WISDEM does not have the fidelity to calculate the effects of internal structural changes on AEP, so AEP is not affected. However, the sensitivity analysis presented in Section 4 reveals negligible AEP sensitivity to changes in joint parameters, so this is not a concern. Although its smaller, less expensive joint yields a lower blade mass and cost than the original BAR-USC, the BAR-USC II 70-m joint design still has heavier, more expensive blades than the rail-transportable monolithic designs from Bortolotti et al. [3], as tabulated in table 1. The higher blade costs are partly from more material, and partly from added manufacturing and assembly costs. To achieve cost parity with the BAR-URC design, each segmented blade of the BAR-USC II 70-m joint design would need to reduce its current nonmaterial manufacturing, assembly, and transportation costs by $82,000, or 16.8% of current blade costs. This said, the gap in costs between the rail-

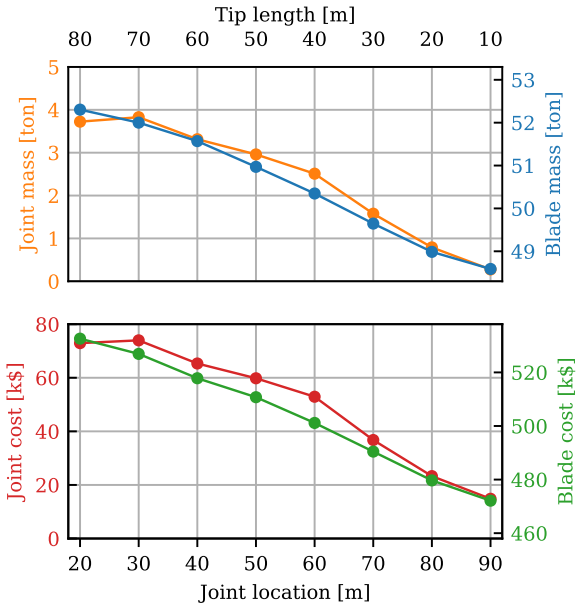

Figure 3. Case study optimization results. The plots have the same y axis scaling on either side, showing that change in joint mass and cost are generally greater than change in blade mass and cost, respectively.

Table 1. Comparison of the turbine designs developed by Bortolotti et al. to the updated BAR-USC II design. Both BAR-USC designs have a 70-m joint location.

	BAR-USC	**BAR-USC II**	**BAR-URC**	**BAR-DRC**
Blade mass (tons)	51.4	**49.6**	41.4	41.4
Blade cost ($K)	528	**490**	453	453
Turbine capital costs ($ kW^{-1})	1,528	**1,502**	1,461	1,460
AEP (GWh)	24.7	**24.7**	24.9	24.7
LCOE ($ MWh^{-1})	37.0	**36.6**	35.7	35.8

transportable and the segmented designs is now narrower thanks to the more accurate joint design model, and future manufacturing and transportation cost modeling should be added to finalize an accurate levelized cost of energy (LCOE) and turbine cost comparison. As blades grow longer and are transported to difficult-to-access locations, transportation cost savings may outweigh added joint costs.

4. Sensitivity analysis

4.1. Sensitivity analysis setup

To determine how mechanical segmentation joint parameters affect blade cost and turbine performance, a sensitivity analysis is performed using the aeroservoelastic framework OpenFAST, with its geometrically exact beam model BeamDyn simulating the blade elastic response. Each OpenFAST run is 720 seconds long, with the first 120 seconds discarded to ignore startup transients. Joint mass, inertia, stiffness, and location are considered. Blade structural mass is a major cost driver. In this design it is driven by tip deflection, which is maximal at design load case (DLC) 1.3, mean wind speed 23 m/s (extreme turbulence). For the rest of the simulations, DLC 1.1 (normal turbulence) is considered, with wind speeds varied between the cut-in and cut-out speeds with steps of 2 m/s. A Weibull distribution of wind speeds for class IIIA and $U_{avg} = 7.5$ m/s was used to weight the individual runs to calculate AEP for DLC 1.1. DELs of blade root moments and tower base moments, which are design-driving loads, were calculated using the Python package fatpack [16]. Table 2 displays the sensitivity runs performed. For the mass, inertia, and stiffness sensitivity, the joint is located at 70 m and a mass of 1,580 kg is used based on the joint mass found from the WISDEM optimization of a 70-m joint. For the location sensitivity, the joint mass is scaled based on results from WISDEM optimization runs with joints across the blade span. In this joint relationship, mass is proportional to location $^{-1/2}$. Except for the inertia sensitivity, inertia is scaled to match the mass used. Besides the stiffness sensitivity, stiffness is unchanged. Finally, the sensitivity of wind turbine LCOE to segmented blade transportation cost (relative to monolithic blade transportation cost) is calculated using WISDEM.

Table 2. Summary of mechanical joint parameters used in the sensitivity study. **Bold** masses were calculated from WISDEM optimization results at a given location. Inertias were scaled with masses in all except the inertia study. Locations are a subset of the 30 specified blade stations in this design.

Study	**Mass [kg]**	**Inertia multiplier**	**Stiffness multiplier**	**Location [span]**
Mass	[200:200:2000]	Scales w/mass	1	70%
Inertia	**1580**	[1:0.5:5.5]	1	70%
Stiffness	**1580**	Scales w/mass	[0.2:0.2:1, 1.5:0.5:5]	70%
Location	**[3720 3830 3310 2960 2510 1580 790]**	Scales w/mass	1	[21:3.45:79%]

4.2. Sensitivity analysis results

Sensitivity results are normalized by the first value in each sensitivity and displayed in figures 4 and 5. Values with $< 1\%$ spread were deemed insensitive and not shown. AEP is insensitive to all varied parameters. Of these, joint mass has the greatest effect on tip deflection, tower base

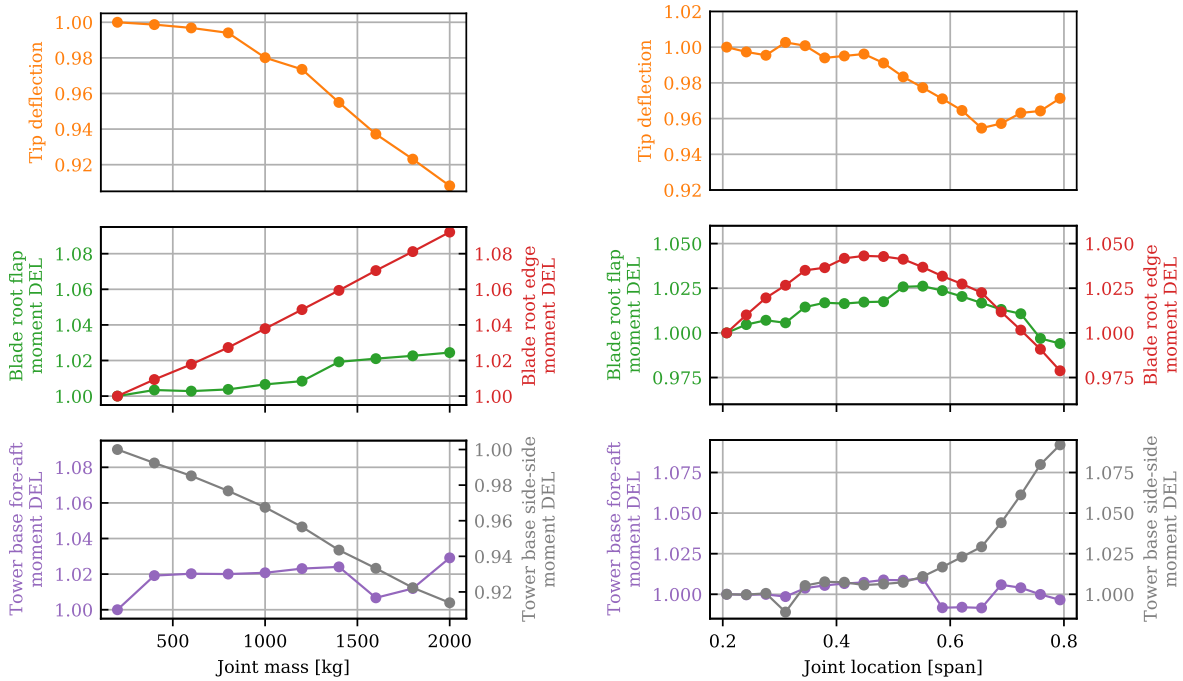

Figure 4. Joint mass (left) and location (right) sensitivities, normalized by the first value.

fore-aft moment DELs, and blade root edge moment DELs, with variations of 10%, 3%, and 9%, respectively. With increased joint mass, blade root moment DELs increase, as expected, and tip deflection decreases slightly, presumably due to increased centrifugal forces pulling the rotor forward, away from the tower. Curiously, tower base side-side moment DEL decreases with increasing joint mass. This decrease will be investigated in future work and is likely related to a mild aeroelastic instability of the rotor.

Joint location (with joint mass and inertia scaled according to results from the WISDEM optimization) has the greatest effect on tower base side-side moment DEL, which increases with blade span and has a variation of about 11%. It also has the greatest effect on blade root flap moment DELs, with a variation of over 3%. Blade root moments are at a maximum with a midspan joint, and tip deflection reaches a minimum with a joint around 66% of the blade span.

Blade root moment DELs increase with joint stiffness. As expected, a stiffer blade joint (which yields a stiffer blade overall) reduces tip deflection. Joint inertia has negligible effect on all outputs considered. Finally, the sensitivity of LCOE to joint cost is linear, at \$0.109/MWh per \$10,000 joint cost. So, the nonmaterial joint costs (manufacturing, assembly, transportation) used in the case study increase wind turbine LCOE by \$0.12/MWh for a 90% span joint to \$0.20/MWh for a 20% span joint over the monolithic blade.

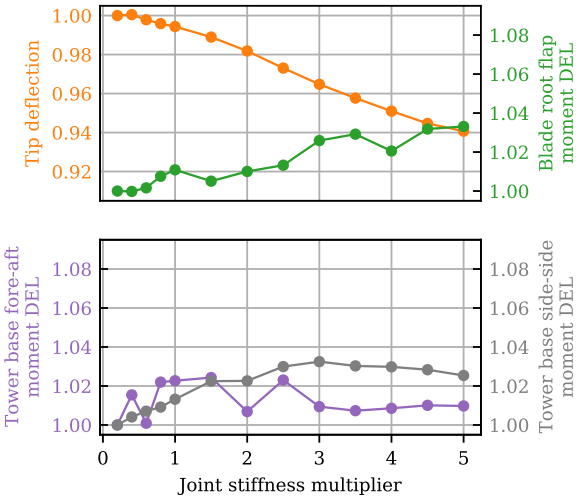

Figure 5. Joint stiffness sensitivity, normalized by the first value.

5. Conclusions

As wind turbine blades grow ever larger, segmentation has the potential to increase blade access to certain regions and reduce blade transportation costs. A detailed mechanical joint model was developed and integrated into the open-source WISDEM framework, supporting the future research and design of segmented blades. The joint model coupled with WISDEM designs segmented blades that have lighter joints and lower blade mass than previous segmented blade BAR designs, although they are still heavier and more expensive than rail-transportable monolithic BAR designs. The sensitivity analysis in this study revealed that joint mass, stiffness, and location may have significant (up to 11%) effects on tower base moments, blade root moments, and tip deflection, which are major structural design drivers. Joint inertia has negligible effects. As expected, joint parameters do not significantly affect AEP.

Future research needs include analyzing the modal impacts of the joint on the blade, developing transportation models and joint manufacturing/assembly cost models to further refine the cost calculations, adding different joint options to the model according to areas of research interest (such as adhesive joints, chordwise joints, and multiple spanwise joints for extremely large blades [17]), increasing the detail of joint geometry and stiffness, including edgewise and torsional loading in the joint design, validating the mechanical method used by the existing joint model with a high-fidelity finite element analysis model, increasing the autonomy of the code to find optimal bolt sizes and joint locations, performing a break-even study to determine at what length segmented blades become more cost-effective than monolithic blades, and investigating why increasing joint mass decreased the tower base side-side moment DEL in the sensitivity study.

Acknowledgements

The authors would like to thank Ryan Clarke and Josh Paquette of Sandia National Laboratories for assistance with developing the joint model. This work was authored by the National Renewable Energy Laboratory, operated by Alliance for Sustainable Energy, LLC, for the U.S. Department of Energy (DOE) under Contract No. DE-AC36-08GO28308. Funding provided by U.S. Department of Energy Office of Energy Efficiency and Renewable Energy Wind Energy Technologies Office. The views expressed in the article do not necessarily represent the views of DOE or the U.S. Government. The U.S. Government retains and the publisher, by accepting the article for publication, acknowledges that the U.S. Government retains a non-exclusive, paid-up, irrevocable, worldwide license to publish or reproduce the published form of this work, or allow others to do so, for U.S. Government purposes. A portion of the research was performed using computational resources sponsored by the U.S. Department of Energy's Office of Energy Efficiency and Renewable Energy and located at the National Renewable Energy Laboratory.

References

[1] Mathijs Peeters, Gilberto Santo, Joris Degroote, and Wim Van Paepegem. The Concept of Segmented Wind Turbine Blades: A Review. *Energies*, 10(8):1112, August 2017. Number: 8 Publisher: Multidisciplinary Digital Publishing Institute.

[2] Dayton A. Griffin and Thomas D. Ashwill. Blade System Design Studies Volume I: Composite Technologies for Large Wind Turbine Blades. Technical Report SAND2002-1879, Sandia National Lab. (SNL-NM), Albuquerque, NM (United States); Sandia National Lab. (SNL-CA), Livermore, CA (United States), July 2002.

[3] Pietro Bortolotti, Nick Johnson, Nikhar J Abbas, Evan Anderson, Ernesto Camarena, and Joshua Paquette. Land-based wind turbines with flexible rail transportable blades – Part I: Conceptual design and aeroservoelastic performance. page 22, 2021.

[4] Nicole Mendoza, Roland Feil, Nick Johnson, and Benjamin Anderson. Conceptual Designs of the Structure of Inflatable Blades for Enabling Larger Turbines. January 2021.

[5] Chandrashekhar Bhat, Dilifa J Noronha, and Faber A Saldanha. Structural Performance Evaluation of Segmented Wind Turbine Blade through Finite Element Simulation. 9(6):10, 2015.

[6] Zhiwen Qin, Lei Zhang, Ke Yang, Jihui Wang, Caicai Liao, and Jianzhong Xu. Determining Division Location for Sectional Wind Turbine Blades. *Energies*, 10(9):1404, September 2017.
[7] Zhiwen Qin, Jihui Wang, Ke Yang, Guangan Yu, Yu Xu, and Jianzhong Xu. Design and nonlinear structural responses of multi-bolted joint composite box-beam for sectional wind turbine blades. *Composite Structures*, 206:801–813, December 2018.
[8] Faber A. Saldanha, V. Venkateswara Rao, J. Christopher, and Raviraja Adhikari. Investigations on Concepts for Modularizing a Horizontal Axis Wind Turbine Blade. American Society of Mechanical Engineers Digital Collection, February 2014.
[9] E. Saenz, I. Nuin, R. Montejo, and J. Sanz. Development and validation of a new joint system for sectional blades. *Wind Energy*, 18(3):419–428, 2015. _eprint: https://onlinelibrary.wiley.com/doi/pdf/10.1002/we.1704.
[10] Nathan Post, Derek Berry, David Snowberg, Andrew Ning, and Derek Petch. Conceptual Joint Design and Incremental Costing and Weight.pdf. Technical report, NREL, September 2013.
[11] openFAST Documentation, November 2021.
[12] WISDEM Documentation, 2019.
[13] Richard G. Budynas and J. Keith Nisbett. *Shigley's mechanical engineering design*. McGraw-Hill series in mechanical engineering. McGraw-Hill, New York, NY, 9. ed edition, 2011.
[14] Pietro Bortolotti, Kristian Dixon, Evan Gaertner, Megan Rotondo, and Garrett Barter. An efficient approach to explore the solution space of a wind turbine rotor design process. *Journal of Physics: Conference Series*, 1618(4):042016, September 2020. Publisher: IOP Publishing.
[15] Kevin J. Smith and Dayton Griffin. Supersized Wind Turbine Blade Study: R&D Pathways for Supersized Wind Turbine Blades. March 2019.
[16] Gunnstein Thomas Frøseth. Gunnstein/fatpack, January 2022. original-date: 2017-12-10T17:10:40Z.
[17] Alejandra S Escalera Mendoza, Shulong Yao, Mayank Chetan, and Daniel Todd Griffith. Design and analysis of a segmented blade for a 50MW wind turbine rotor. *Wind Engineering*, page 0309524X211069393, January 2022. Publisher: SAGE Publications.